ADVANCED ELECTRONIC MATERIALS
www.advelectronicmat.de

2D Material-Based Vertical Double Heterojunction Bipolar Transistors with High Current Amplification

*Geonyeop Lee, Stephen J. Pearton, Fan Ren, and Jihyun Kim**

The heterojunction bipolar transistor (HBT) differs from the classical homojunction bipolar junction transistor in that each emitter-base-collector layer is composed of a different semiconductor material. 2D material (2DM)-based heterojunctions have attracted attention because of their wide range of fundamental physical and electrical properties. Moreover, strain-free heterostructures formed by van der Waals interaction allows true bandgap engineering regardless of the lattice constant mismatch. These characteristics make it possible to fabricate high-performance heterojunction devices such as HBTs, which have been difficult to implement in conventional epitaxy. Herein, NPN double HBTs (DHBTs) are constructed from vertically stacked 2DMs (n-MoS_2/p-WSe_2/n-MoS_2) using dry transfer technique. The formation of the two P–N junctions, base-emitter, and base-collector junctions, in DHBTs, was experimentally observed. These NPN DHBTs composed of 2DMs showed excellent electrical characteristics with highly amplified current modulation. These results are expected to extend the application field of heterojunction electronic devices based on various 2DMs.

Heterostructures are widely employed in semiconducting devices to take advantage of band-structure engineering effects that lead to significantly improved carrier confinement and injection.[1] This leads to a wide variety of device performance advantages in photonic and electronic devices and over their homojunction analogs, including higher gains in transistors or brighter light outputs from the photonic devices.[2] This approach is also advantageous for mitigating the problems related to the reduction of carrier mobility as the doping concentration increases in homojunctions by separating the carriers from the dopants and also in situations where efficient bipolar doping is difficult. As a result, heterostructures have been applied to various types of semiconductor devices, such as lasers, solar cells, high electron mobility transistors, and heterojunction bipolar transistors (HBTs).[3–6] Notably, with a bipolar junction transistor, which is a three-terminal transistor fabricated by connecting two P–N homojunction diodes, there is a trade-off between the current gain and high-frequency ability because of these problems.[3,7] In sharp contrast, HBTs realized using the heterostructure can avoid these trade-offs and improve device performance.[8] HBTs, due to their high power efficiency, uniformity of threshold voltage, and low 1/f noise characteristics, have been widely used in high power amplifiers and high frequency switching devices.[3] It is challenging to realize high-quality hetero-interfaces in heterojunction devices, including HBTs owing to the various growth limitations involving mitigation of diffusion of both dopants and lattice elements. If present, these constraints contribute to performance degradation or even the complete loss of the benefits of incorporating the heterojunction.[3] For instance, III–V compound semiconductors such as GaAs/AlGaAs and GaN/AlGaN used in conventional heterojunction-based devices require high vacuum and high-cost growth equipment such as metalorganic vapor deposition (MOCVD) and molecular beam epitaxy (MBE). This growth is difficult to achieve when the difference of the lattice constants is too significant. Additionally, obstacles such as dislocation defects, strain caused by lattice mismatch, cross-contamination, and inter-diffusion are difficult to overcome. These problems cause device performance deterioration in the form of increased leakage current, a decrease of breakdown voltage, and an increase of recombination rate in HBT devices.[1–3]

2D materials (2DMs) have been studied in various fields over the past decade because of their excellent electrical, thermal, and mechanical properties.[9–13] In particular, heterostructures based on 2DMs have attracted interest because of their weak interlayer bonding, quantum effect, and tunneling, which are differentiated from conventional 3D bulk materials.[10,14] Weak van der Waals interactions of 2DMs can not only easily separate each layer, but can also layer materials regardless of lattice mismatch.[11] Additionally, because 2DMs have a sharp interface and no dangling bonds, heterostructures using 2DMs can solve problems such as atomic diffusion and dislocation propagation, which have been regarded as limitations of existing 3D bulk materials.[11,12] Selection of 2DMs provides

G. Lee, Prof. J. Kim
Department of Chemical and Biological Engineering
Korea University
Seoul 02841, Korea
E-mail: hyunhyun7@korea.ac.kr
Prof. S. J. Pearton
Department of Materials Science and Engineering
University of Florida
Gainesville, FL 32611, USA
Prof. F. Ren
Department of Chemical Engineering
University of Florida
Gainesville, FL 32611, USA
The ORCID identification number(s) for the author(s) of this article can be found under https://doi.org/10.1002/aelm.201800745.

DOI: 10.1002/aelm.201800745

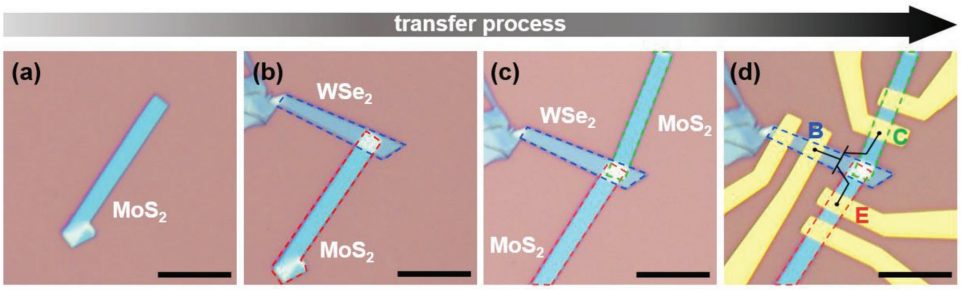

Figure 1. Optical microscope images a–d) showing the process of fabricating an NPN DHBT using the exfoliated MoS_2 and WSe_2 flakes in the order $MoS_2/WSe_2/MoS_2$. d) Definition of Ti/Au electrodes for MoS_2 and Pt/Au electrodes for WSe_2 flakes. Note that two electrodes were defined on each flake to confirm the Ohmic contact. Scale bars of all figures represent 10 μm.

latitude in achieving specific electrical and optical properties because each material has a different energy bandgap, electron affinity, and carrier mobility, thereby allowing the design of desired devices to be fine-tuned without being limited by lattice constants.[11,12,15] Roy et al. demonstrated the negative differential resistive characteristics of the Esaki diode in a hetero WSe_2-MoS_2 junction and analyzed its electrical and optical properties.[16] Liu et al. fabricated P–N diodes composed of black phosphorus and MoS_2 and proved that diode characteristics can be changed according to the thickness of black phosphorus.[17] Although studies on heterostructures based on various 2DMs have been carried out, the research is still limited to fundamental structures, such as a single P–N junction diode. Even though three-terminal active devices, like HBTs and junction field-effect transistors, are more useful than two-terminal devices from the point of view of the multiple applications ranging from signal applications to the design of digital logic, those have not yet been widely studied.[13]

This study demonstrates the highly amplified current modulation of a double HBT (DHBT), composed of vertically stacked 2DMs. MoS_2, used as an n-type emitter and collector, was stacked vertically with WSe_2, a p-type base, to fabricate an NPN DHBT at room temperature and atmospheric pressure. MoS_2 and WSe_2 are extensively used as 2D semiconductor materials. They have excellent electrical properties of electron or hole mobility and possess a tunable bandgap depending on their thickness, which enables easy bandgap engineering for the HBTs. In addition, several researchers have reported a WSe_2–MoS_2 type II P–N junction, which has a potential for HBTs.[16,18] The NPN structure was selected because it has been reported that junction barrier for the electron is slightly lower than that for the hole carrier in WSe_2-MoS_2 junction .[19] Lateral type HBTs fabricated with 2DMs have been reported by Lin et al. but vertical structure can reduce the recombination loss in the base region more efficiently than the lateral type, making very thin 2D materials even more advantageous.[1,3,7,20] Double heterojunction structure was adopted because it can help avoid the difficulty of self-doping and the performance trade-off problem because of doping in contrast to a single heterojunction structure. The presence of heterojunctions in the fabricated DHBTs was confirmed through systematic analysis using transmission electron microscopy (TEM), Raman microscopy, atomic force microscopy (AFM), and electrical measurements. Our DHBT devices showed excellent electrical properties in common-emitter and common-base mode. In particular, the high current gain (β) obtained through the Gummel plot was comparable to those of commercialized III–V thin film semiconductor HBTs.

Figure 1 shows optical microscope images that depict the fabrication process of DHBTs based on 2D materials via van der Waals epitaxy (dry transfer technique). The bottom n-type MoS_2 flake was first transferred onto the SiO_2/Si (300 nm/525 μm) substrate (Figure 1a). Then, the p-type WSe_2 and n-type MoS_2 flakes were stacked vertically onto the previously transferred flake, using a micromanipulator, in the order NPN (Figure 1b,c). This procedure separated the top MoS_2 from the bottom MoS_2 flakes with a WSe_2 layer. A Ti/Au electrode and Pd/Au electrode were defined for the MoS_2 (emitter or collector) and WSe_2 (base), respectively, using standard electron-beam lithography, electron-beam evaporation, and lift-off processes (Figure 1d). **Figure 2**a shows a schematic of the fabricated NPN DHBT, which was fabricated by stacking two MoS_2 (n-type) flakes and a WSe_2 (p-type) flake vertically, in the order NPN, using a drytransfer technique. Here, the top or bottom MoS_2 acts as an emitter (collector) or a collector (emitter), respectively, and WSe_2 in the middle layer is used as a base material. Figure 2b,c shows the AFM images and height profile of one of the fabricated devices (shown in Figure 1). The green, blue, and red dotted lines in Figure 2b indicate the bottom MoS_2, WSe_2, and top MoS_2 flakes, respectively. The 2D flakes were ≈9, ≈8, ≈10 nm thick, respectively. 2DM flakes of similar thickness were used for other samples, and the maximum thickness did not exceed 50 nm. A cross-sectional TEM image was obtained using another fabricated DHBT sample to confirm the quality and structure of the heterostructure vertically stacked in $MoS_2/WSe_2/MoS_2$. A TEM image (Figure 2d) and the corresponding energy-dispersive X-ray microscopy (EDX) mapping images (Figure S1, Supporting Information) show the well-formed heterostructure without strain or bubbles. This indicates that van der Waals epitaxy can prevent the lattice mismatch that occurs because of the 5.53% larger lattice constant of WSe_2 compared to that of MoS_2.[21] The Raman spectra of the $MoS_2/WSe_2/MoS_2$ heterostructure are shown in Figure 2d. The peaks at ≈382 and ≈408 cm^{-1} correspond to the E^1_{2g} and A_{1g} phonon modes of MoS_2, respectively, and the peaks at ≈248 and ≈257 cm^{-1} correspond the E^1_{2g} and A_{1g} phonon modes of WSe_2, respectively.[22,23] The Raman peaks of MoS_2 in the area where all three flakes overlapped were slightly broader and shifted as previous studies reported, indicating

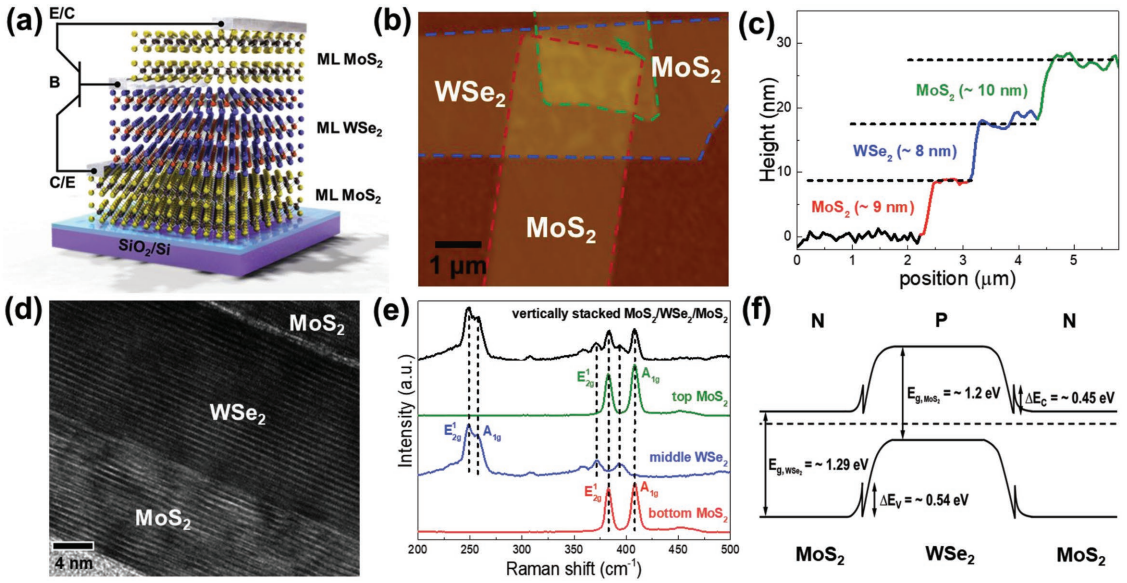

Figure 2. a) Schematic of an NPN DHBT grown on SiO_2/Si substrate. b) AFM image of the DHBT device represented in Figure 1. The red, blue, and green dotted lines indicate the bottom MoS_2, WSe_2, and top MoS_2 flakes, respectively. c) AFM height profile of a MoS_2/WSe_2/MoS_2 DHBT. d) Cross-sectional TEM image of the stacked MoS_2/WSe_2/MoS_2. e) Raman spectra of the bottom MoS_2, middle WSe_2, and top MoS_2. The black line indicates the Raman spectra from the position at which three flakes overlap. f) Band structure of the MoS_2/WSe_2/MoS_2 NPN DHBT.

that charge transfer occurred and a depletion layer was formed at the MoS_2/WSe_2 van der Waals heterojunction.[24–27] The energy band structure of the NPN DHBT is shown in Figure 2f. Several previous studies have shown that abrupt type II P–N junctions form in multilayer WSe_2-MoS_2 structures.[20,28–30] In bulk P–N junctions of these two materials, charge transfers occur because of the diffusion of the majority carriers. As a result, a depletion layer is formed at the WSe_2 and MoS_2 interfaces. A band offset with ΔE_C ($\chi_{WSe_2} - \chi_{MoS_2} = 0.45$ eV) and ΔE_V ($(E_{g,MoS_2} - E_{g,WSe_2}) - (\chi_{MoS_2} - \chi_{WSe_2}) = 0.54$ eV) obtained from Anderson's rule indicates that the heterojunction between MoS_2 and WSe_2 is suitable for HBT operation. The band structure shown in Figure 2f has a symmetric shape, but it is expected that an asymmetric band structure will be applied during actual operation of the device because of the orientation of top or bottom MoS_2 and WSe_2 and different thicknesses of the top and bottom MoS_2 flakes.[31] The base thicknesses and depletion states of the NPN DHBT devices are critical for improving the performance of a device.[3,32] Although the depletion model in 2D-based P–N junctions is not fully understood, we can estimate the base thickness suitable for vertical NPN DHBT devices by calculating the width of the depletion layer using a conventional depletion model of the P–N junction. The width of the depletion layer in the p-type material can be calculated using the following equation

$$W_d = \sqrt{\frac{2N_d\varepsilon_1\varepsilon_2 V_{bi}}{qN_a(\varepsilon_1 N_a + \varepsilon_2 N_d)}} \quad (1)$$

where q is the charge of an electron, N_d and N_a are the donor and acceptor carrier density, respectively, and ε_1 and ε_2 are the permittivity constants of MoS_2 and WSe_2, respectively, and V_{bi} is the built-in potential.[2] The carrier densities of the MoS_2 and WSe_2 were reported to be a few 10^{12} cm^{-2}, and thicknesses of a few nm to several tens of nm were obtained by calculating the depletion width.[27,29,33] For example, if we assume that N_d, N_a, ε_1, ε_2, and V_{bi} have values of 3.4×10^{18} cm^{-3} ($n = 3.1 \times 10^{12}$ cm^{-2}), 4.8×10^{17} cm^{-3} ($p = 3.8 \times 10^{11}$ cm^{-2}), 12.8, 11.7, and 0.33 eV, respectively, then the estimated depletion layer width is around 29.2 nm.[27] The conventional depletion model is based on the study of intentionally doped semiconductor materials through diffusion theory; therefore, it is difficult to apply it perfectly to other materials, like 2DMs.[34] The depletion widths of van der Waals structures are known to be smaller than those predicted by conventional depletion models owing to the strong interfacial charge coupling.[27,35] Doan et al. reported that a device was not completely turned off in the WSe_2 channel, which was expected to be fully depleted via the conventional depletion model, in devices composed of WSe_2/MoS_2 junctions.[27] Therefore, the actual depletion width of WSe_2 in our NPN DHBTs might be smaller than the expected value of tens of nanometers and thus may not be completely depleted.

Electrical measurements were performed on the NPN vertical DHBTs under ambient conditions. A representative device was shown in this work, while five fabricated devices exhibited similar electrical characteristics (the optical microscope image and electrical properties of one of the other fabricated devices are included in Figure S2 in the Supporting Information). **Figure 3**a,b represents the typical *I*–*V* characteristics of each P–N junction of our DHBTs (the insets show the *I*–*V* characteristics on a log scale). The fabrication process and optical microscope images of the corresponding device are shown in Figure S3 in the Supporting Information Typical rectifying behaviors of the P–N junction were observed at the base-emitter (Figure 3a) and base-collector (Figure 3b) between p-WSe_2 and n-MoS_2. Rectification ratios ($|I_{+15\ V}/I_{-15\ V}|$) were ≈120 and ≈230, respectively, similar to those reported by

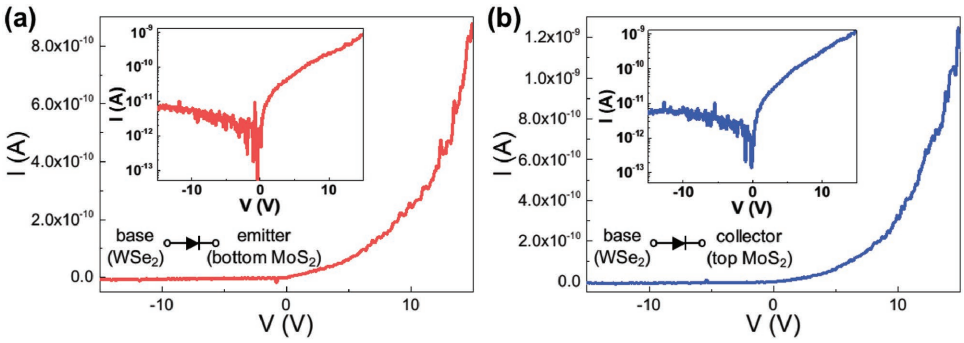

Figure 3. Current–voltage (*I–V*) characteristics of a) base-emitter (WSe_2-top MoS_2) and b) base-collector (WSe_2-bottom MoS_2) heterojunctions. The insets show *I–V*s on a log scale.

the previous studies.[18,28] The ideality factor was obtained using the following equation

$$I = I_0 \left(e^{qV/nkT} - 1\right) \quad (2)$$

where I is current through the diode, V is the voltage across the diode, I_0 is dark saturation current, n is the ideality factor, k is the Boltzmann constant, and T is the absolute temperature.[36] The ideality factors of the base-emitter and base-collector were ≈10 and ≈5, respectively, which are much higher than those of the ideal P–N junction.[34] The transport of carriers in abrupt heterojunctions is usually controlled by thermionic field emission.[37] In our devices, the ideality factor was higher because of tunneling currents, similar to what previous studies have reported.[38,39] Problems such as polymer residue, the formation of an edge defect, and strain, which occur during the fabrication process, might have caused the high ideality factors.

The electrical characteristics of an NPN DHBT in common-emitter mode are represented in **Figure 4**. Here, the base-emitter (WSe_2-bottom MoS_2) was forward-biased and the base-collector (WSe_2-top MoS_2) was reverse-biased when the emitter was grounded. Figure 4a shows the input characteristics of an NPN device, which indicate the dependence of the base current on V_{BE} when the voltage bias was applied in the forward direction. A shape similar to the forward *I–V* characteristics of a P–N junction diode was observed. The base current decreased as V_{BE} increased and saturation began at the V_{CB} = +4 V. This indicates that the base current can be independent of the band shape because of the potential difference between the collector and emitter above V_{CB} = +4 V. Figure 4b shows the Gummel plot characteristics, where the measurement was performed

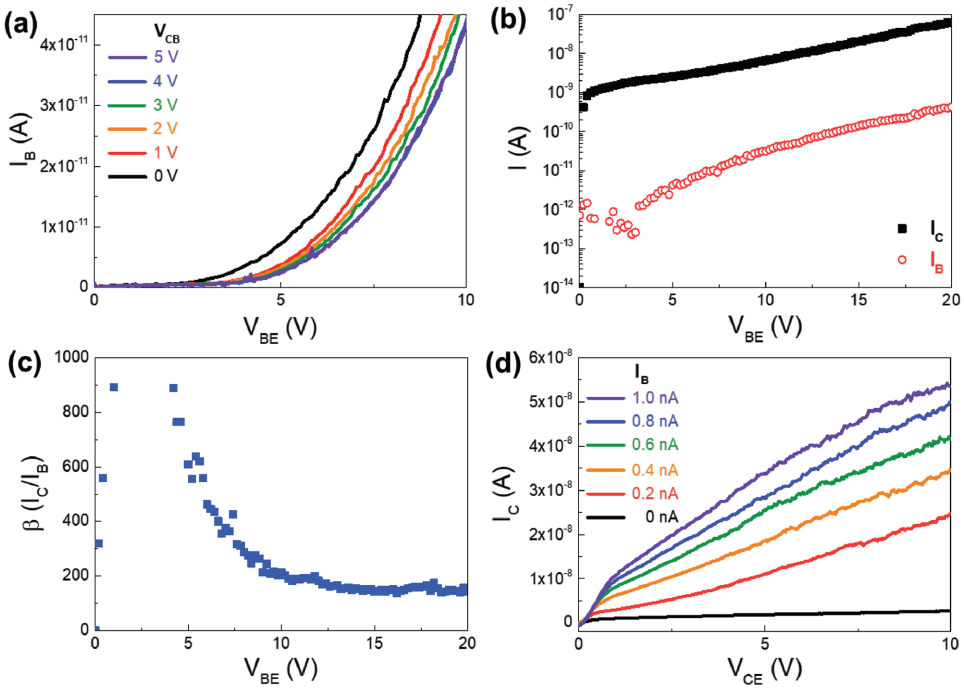

Figure 4. a) Electrical input characteristics of NPN vertical DHBT under different V_{CE} conditions. b) Gummel plot for the measured NPN DHBT in common emitter configuration when the collector and emitter are shorted (V_{CB} = 0 V). c) Corresponding current gain (β) in common emitter mode as a function of V_{BE}. d) The output characteristics of NPN vertical DHBT according to the base current.

Table 1. Comparison of device performance and properties between this work and other previously reported HBT devices.

Material	Type	β	J_c [A cm^{-2}]	Structure	Reference
AlGaAs/GaAs	NPN	100	–	Vertical (3D)	[44]
GaN/InGaN	NPN	105	6.5 k	Vertical (3D)	[45]
AlGaN/GaN	PNP	25	2.05 k	Vertical (3D)	[46]
GaN/InGaN	NPN	90	12.3 k	Vertical (3D)	[47]
Si/MoS_2/GaTe	PNP	7	70	Vertical (2D/3D)	[49]
Si/MoS_2/ITO	HET	4	4	Vertical (2D/3D)	[50]
MoS_2/WSe_2	NPN	3	0.0126	Lateral (2D)	[20]
MoS_2/WSe_2	NPN	150	1.34	Vertical (2D)	This work

using the conventional method that shorts the collector-to-base voltage (V_{CB} = 0).[3,7] The gap of current between the collector current (I_C) and the base current (I_B) shown in the Gummel plot clearly shows that the collector current was amplified by the input of I_B. Current gain (β) in the common-emitter mode from the Gummel plot is shown in Figure 4c and is defined as $\beta = I_C/I_B$.[7] An abnormally high β was observed in the low V_{BE} region (low I_B region), which might be caused by the leakage current because of the Schottky-like Ohmic contact in the base region of the device.[40–43] The average value of β above 10 V is around 150 with a collector current density (J_C) of 1.34 A cm^{-2}, which is comparable to that of conventional III–V semiconductor devices.[20,44–50] The comparison between previously reported devices and our fabricated device is shown in **Table 1**. This shows that our results not only increase the practical possibility of 2DM-based heterojunction devices but also satisfy the performance criteria of devices grown by conventional epitaxy. Note that the fabrication process and thickness of our DHBT have not been optimized yet, which indicates that there is room for improvement in the device performance. We also measured the output characteristics from I_B = 0 to 1.0 nA with a step size of 0.2 nA (Figure 4d). It was confirmed that the collector current of the device amplified when the base current was injected while applying V_{CE} in the positive direction. On the other hand, if $\beta = I_C/I_B$ was applied as is, the value of I_{C0} (I_B = 0) should be included in I_C as the emitter-to-collector leakage current. Therefore, β in the output characteristics should be modified as $\beta = \Delta I_C(=I_C - I_{C0})/I_B$. As a result, β had values of ≈100 and ≈55 when I_B = 0.2 and 1.0 nA, respectively, which is consistent with the Gummel plot. Figure S4 in the Supporting Information shows that the output characteristics exhibited higher current gain after the I_B step was adjusted to 50 pA. It is assumed that β fall-off with increasing base current was caused by the Kirk effect or emitter crowding effect.[1,3] The information about the values of $\beta = \Delta I_C(=I_C - I_{C0})/I_B$ and the thicknesses of flakes for each fabricated device are shown in Figure S5 and Table S1 in the Supporting Information.

Furthermore, electrical characteristics in the common-base mode were measured, as shown in **Figure 5**a, which is similar to that of the P–N diode in the forward direction. The emitter current (I_E) increased as V_{CB} increased. This implies that the carrier movement at the emitter-base junction was affected by the band alignment change of the collector-base junction. Figure 5b shows the output characteristics in common-base mode, where the measurements were performed by injecting I_E (=I_{BE}) from 0 to 2 nA with 0.4 nA step increments. The base was grounded while V_{CB} was positive and V_{EB} was negative. It was observed that the current modulation without amplification was the same as the operation of general HBTs. I_C, when I_E = 0 nA (I_{C0}), was close to zero. The current gain (α) in common-base mode can be defined as $\alpha = I_C/I_E$.[7] Because I_{C0} was very small, consideration of ΔI_C was not necessary, and the value of α derived from the saturation region is close to 1. These results indicate that recombination at the base region did not significantly affect the loss of carriers moving from emitter to collector. This suggests that 2DMs can provide high-quality heterojunctions with a very thin base material, which significantly contributes to the performance of the electronic devices. Our results show the potential for device fabrication using 2DMs, which has several advantages, such as bandgap engineering without consideration of lattice constant, absence of memory effects during growth, and existence of various types of 2DMs.[48]

We demonstrated the fabrication of vertical NPN DHBTs using 2DMs stacking and showed efficient current amplification and modulation. Two MoS_2 flakes, as an emitter and collector and a WSe_2 flake as a base, were vertically aligned in the order $MoS_2/WSe_2/MoS_2$. The formation of the hetero P–N junction at the base-emitter and base-collector interfaces was analyzed using Raman spectra, AFM, TEM, and diode *I–V* characteristics. Amplified current-modulation and saturation characteristics of NPN DHBTs in common-emitter and common-base mode were observed. The maximum current gain (β) in common-emitter mode from the Gummel plot of the fabricated sample was ≈150, which is comparable to that

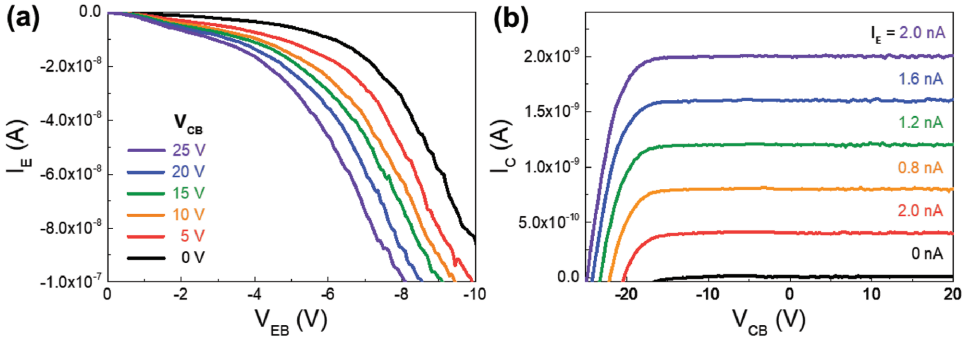

Figure 5. a) Input characteristics of NPN vertical DHBT according to V_{CB}. b) Output characteristics of NPN vertical DHBT according to I_E.

of conventional HBTs based on III–V semiconductors grown under a high vacuum condition. Excellent current switching in common-base mode was also obtained. This approach is appropriate for producing rectifiers and amplifiers that meet the performance criteria established for devices produced by conventional epitaxy and processing. We believe that our study allows the fabrication of structures having new functionalities and high-performance, which was not previously possible because of lattice-mismatch, and the requirements of high-vacuum equipment.

Experimental Section

Device Fabrication: The n-type (MoS_2) or p-type (WSe_2) flakes that make up the HBTs were mechanically exfoliated from each bulk crystal (MoS_2: graphene supermarket, WSe_2: HQ graphene) using an adhesive tape and then were transferred to transparent gel film. Then, two n-type MoS_2 flakes and one p-type WSe_2 flake were stacked vertically onto the SiO_2/Si (300 nm/525 µm) substrate, using a micromanipulator, in the order NPN. A Ti/Au electrode (50/100 nm) and Pd/Au electrode (50/100 nm) were defined for MoS_2 and WSe_2, respectively, using standard electron-beam lithography, electron-beam evaporation, and lift-off processes. Oxygen plasma treatment (50 W, 25 sccm for 10–30 s) was used in a small area around the WSe_2/electrodes to obtain a better Ohmic contact.[25] Two electrodes were defined on each NPN flake to confirm the successful injection of the charge carriers.

Device Measurements: The thickness of each flake was measured using an AFM (Bruker Corp.) in tapping mode. Raman spectra were obtained using a micro-Raman instrument with a 532 nm diode-pumped solid-state laser (Omicron) under a back-scattering geometry. The heterostructure stacked within the NPN MoS_2/WSe_2/MoS_2 flakes was investigated with a scanning transmission electron microscope (STEM; JEM-2100F, JEOL); the specimen was prepared using the focused ion beam (FIB) technique (Quanta 2003D, FEI) after a carbon and platinum coating was applied to protect the sample. The electrical properties of the HBTs were measured under an ambient air using a semiconductor parameter analyzer (4155C, Agilent) connected to a probe station.

Supporting Information

Supporting Information is available from the Wiley Online Library or from the author.

Acknowledgements

The research at Korea University was supported by National Research Foundation of Korea. It was funded by the Technology Development Program to Solve Climate Changes of the National Research Foundation, funded by the Ministry of Science and ICT (NRF-2017M1A2A2087351), the Korea Institute of Energy Technology Evaluation and Planning (KETEP), granted financial resource from the Ministry of Trade, Industry & Energy, Korea (20172010104830), and the Korea University Graduate Student Junior Fellow Research Grant.

Conflict of Interest

The authors declare no conflict of interest.

Keywords

heterojunction bipolar transistor, molybdenum disulfide, P–N junction, tungsten diselenide, 2D materials

Received: October 22, 2018
Revised: November 30, 2018
Published online: December 27, 2018

[1] B. G. Streetman, S. Banerjee, *Solid State Electronic Devices*, Pearson Prentice Hall, Upper Saddle River, NJ, USA **2006**.
[2] J. S. Yuan, *SiGe, GaAs, and InP Heterojunction Bipolar Transistors*, Wiley, New York, NY, USA **1999**.
[3] W. Liu, *Handbook of III–V Heterojunction Bipolar Transistors*, Wiley, New York, NY, USA **1998**.
[4] H. Kressel, M. Ettenberg, I. Ladany, *Appl. Phys. Lett.* **1978**, *32*, 305.
[5] Y. Kwon, J. Seo, Y. Kang, D. Kim, J. Kim, *Opt. Express* **2018**, *26*, A30.
[6] S. Yoshida, H. Ishii, J. Li, D. Wang, M. Ichikawa, *Solid-State Electron.* **2003**, *47*, 589.
[7] G. W. Neudeck, *The Bipolar Junction Transistor*, Addison-Wesley, MA, USA **1989**.
[8] H. Kroemer, *Proc. IEEE* **1982**, *70*, 13.
[9] R. Mas-Ballesté, C. Gómez-Navarro, J. Gómez-Herrero, F. Zamora, *Nanoscale* **2011**, *3*, 20.
[10] K. S. Novoselov, A. Mishchenko, A. Carvalho, A. H. Castro Neto, *Science* **2016**, *353*, aac9439.
[11] A. K. Geim, I. V. Grigorieva, *Nature* **2013**, *499*, 419.
[12] C.-H. Lee, G.-H. Lee, A. M. van der Zande, W. Chen, Y. Li, M. Han, X. Cui, G. Arefe, C. Nuckolls, T. F. Heinz, J. Guo, J. Hone, P. Kim, *Nat. Nanotechnol.* **2014**, *9*, 676.
[13] Y. Liu, N. O. Weiss, X. Duan, H.-C. Cheng, Y. Huang, X. Duan, *Nat. Rev. Mater.* **2016**, *1*, 16042.
[14] M. Huang, S. Li, Z. Zhang, X. Xiong, X. Li, Y. Wu, *Nat. Nanotechnol.* **2017**, *12*, 1148.
[15] M.-H. Chiu, W.-H. Tseng, H.-L. Tang, Y.-H. Chang, C.-H. Chen, W.-T. Hsu, W.-H. Chang, C.-I. Wu, L.-J. Li, *Adv. Funct. Mater.* **2017**, *27*, 1603756.
[16] T. Roy, M. Tosun, X. Cao, H. Fang, D.-H. Lien, P. Zhao, Y.-Z. Chen, Y.-L. Chueh, J. Guo, A. Javey, *ACS Nano* **2015**, *9*, 2071.
[17] X. Liu, D. Qu, H.-M. Li, I. Moon, F. Ahmed, C. Kim, M. Lee, Y. Choi, J. H. Cho, J. C. Hone, *ACS Nano* **2017**, *11*, 9143.
[18] J. H. Yu, H. R. Lee, S. S. Hong, D. Kong, H.-W. Lee, H. Wang, F. Xiong, S. Wang, Y. Cui, *Nano Lett.* **2015**, *15*, 1031.
[19] Y. Zhao, W. Yu, G. Ouyang, *J. Phys. D: Appl. Phys.* **2018**, *51*, 015111.
[20] C.-Y. Lin, X. Zhu, S.-H. Tsai, S.-P. Tsai, S. Lei, Y. Shi, L.-J. Li, S.-J. Huang, W.-F. Wu, W.-K. Yeh, *ACS Nano* **2017**, *11*, 11015.
[21] M.-Y. Li, Y. Shi, C.-C. Cheng, L.-S. Lu, Y.-C. Lin, H.-L. Tang, M.-L. Tsai, C.-W. Chu, K.-H. Wei, J.-H. He, *Science* **2015**, *349*, 524.
[22] H. Li, Q. Zhang, C. C. R. Yap, B. K. Tay, T. H. T. Edwin, A. Olivier, D. Baillargeat, *Adv. Funct. Mater.* **2012**, *22*, 1385.
[23] H. Zeng, G.-B. Liu, J. Dai, Y. Yan, B. Zhu, R. He, L. Xie, S. Xu, X. Chen, W. Yao, X. Cui, *Sci. Rep.* **2013**, *3*, 1608.
[24] B. Chakraborty, A. Bera, D. V. S. Muthu, S. Bhowmick, U. V. Waghmare, A. K. Sood, *Phys. Rev. B* **2012**, *85*, 161403.
[25] M. A. Khan, S. Rathi, C. Lee, D. Lim, Y. Kim, S. J. Yun, D. H. Youn, G.-H. Kim, *ACS Appl. Mater. Interfaces* **2018**, *10*, 23961.
[26] Y. Li, C.-Y. Xu, P. Hu, L. Zhen, *ACS Nano* **2013**, *7*, 7795.
[27] M.-H. Doan, Y. Jin, S. Adhikari, S. Lee, J. Zhao, S. C. Lim, Y. H. Lee, *ACS Nano* **2017**, *11*, 3832.
[28] R. Cheng, D. Li, H. Zhou, C. Wang, A. Yin, S. Jiang, Y. Liu, Y. Chen, Y. Huang, X. Duan, *Nano Lett.* **2014**, *14*, 5590.
[29] A. Nourbakhsh, A. Zubair, M. S. Dresselhaus, T. S. Palacios, *Nano Lett.* **2016**, *16*, 1359.

[30] B. Peng, G. Yu, X. Liu, B. Liu, X. Liang, L. Bi, L. Deng, T. C. Sum, K. P. Loh, *2D Mater.* **2016**, *3*, 025020.
[31] K. Zhou, D. Wickramaratne, S. Ge, S. Su, A. De, R. K. Lake, *Phys. Chem. Chem. Phys.* **2017**, *19*, 10406.
[32] D. Ritter, R. Hamm, A. Feygenson, M. Panish, S. Chandrasekhar, *Appl. Phys. Lett.* **1991**, *59*, 3431.
[33] R. Frisenda, A. J. Molina-Mendoza, T. Mueller, A. Castellanos-Gomez, H. S. van der Zant, *Chem. Soc. Rev.* **2018**, *47*, 3339.
[34] K. F. Brennan, A. S. Brown, *Theory of Modern Electronic Semiconductor Devices*, John Wiley, NY, USA **2002**.
[35] X. Zhu, N. R. Monahan, Z. Gong, H. Zhu, K. W. Williams, C. A. Nelson, *J. Am. Chem. Soc.* **2015**, *137*, 8313.
[36] R. F. Pierret, *Semiconductor Device Fundamentals*, Addison-Wesley, Reading, MA, USA **1996**.
[37] K. Yang, J. R. East, G. I. Haddad, *Solid-State Electron.* **1993**, *36*, 321.
[38] Y. Deng, Z. Luo, N. J. Conrad, H. Liu, Y. Gong, S. Najmaei, P. M. Ajayan, J. Lou, X. Xu, P. D. Ye, *ACS Nano* **2014**, *8*, 8292.
[39] P. J. Jeon, S.-W. Min, J. S. Kim, S. R. A. Raza, K. Choi, H. S. Lee, Y. T. Lee, D. K. Hwang, H. J. Choi, S. Im, *J. Mater. Chem. C* **2015**, *3*, 2751.
[40] K.-P. Hsueh, Y.-M. Hsin, J.-K. Sheu, W.-C. Lai, C.-J. Tun, C.-H. Hsu, B.-H. Lin, *Solid-State Electron.* **2007**, *51*, 1073.
[41] C.-T. Pan, R.-J. Hou, Y.-M. Hsin, H.-C. Chiu, *Electron. Lett.* **2009**, *45*, 230.
[42] H. Fang, S. Chuang, T. C. Chang, K. Takei, T. Takahashi, A. Javey, *Nano Lett.* **2012**, *12*, 3788.
[43] M. Zhu, W. Luo, N. Wu, X.-A. Zhang, S. Qin, *Appl. Phys. Lett.* **2018**, *112*, 183102.
[44] K. Lew, S. Yoon, W. Loke, H. Tanoto, C. Dohrman, D. Isaacson, E. Fitzgerald, *J. Vac. Sci. Technol. B: Microelectron. Nanometer Struct.* **2007**, *25*, 902.
[45] Y. Lee, Y. Zhang, H. Kim, S. Choi, Z. Lochner, R. D. Dupuis, J. Ryou, S. Shen, *IEEE Trans. Electron Devices* **2010**, *57*, 2964.
[46] A. Zhang, G. Dang, F. Ren, J. Han, A. Baca, R. Shul, H. Cho, C. Monier, X. Cao, C. Abernathy, *Appl. Phys. Lett.* **2000**, *76*, 2943.
[47] Z. Lochner, H. J. Kim, Y.-C. Lee, Y. Zhang, S. Choi, S.-C. Shen, P. Doug Yoder, J.-H. Ryou, R. D. Dupuis, *Appl. Phys. Lett.* **2011**, *99*, 193501.
[48] M. Yamamoto, S. Nakaharai, K. Ueno, K. Tsukagoshi, *Nano Lett.* **2016**, *16*, 2720.
[49] X. Yan, D. W. Zhang, C. Liu, W. Bao, S. Wang, S. Ding, G. Zheng, P. Zhou, *Adv. Sci.* **2018**, *5*, 1700830.
[50] C. M. Torres, Y.-W. Lan, C. Zeng, J.-H. Chen, X. Kou, A. Navabi, J. Tang, M. Montazeri, J. R. Adleman, M. B. Lerner, Y.-L. Zhong, L.-J. Li, C.-D. Chen, K. L. Wang, *Nano Lett.* **2015**, *15*, 7905.

